Fabrication of Fe_3O_4/MgAl-layered double hydroxide magnetic composites for the effective removal of Orange II from wastewater

Bo Zhu, Lixian Chen, Tianyi Yan, Jiangyan Xu, Yanyu Wang, Min Chen and Hongmei Jiang

ABSTRACT

A facile approach has been developed to construct a composite of magnetic Fe_3O_4 (MNPs) and regular hexagon Mg-Al layered double hydroxide (MNPs/MgAl-LDH) via a two-step hydrothermal method combined with the urea hydrolysis reaction for the removal of Orange II. The scanning electron microscopy, X-ray diffraction and Fourier transform infrared spectroscopy results showed MNPs and MgAl-LDH have been combined successfully, providing the combination of the superior properties of fast separation and high adsorption capacity. The pH values, contact time, initial dye concentration and temperature were investigated in detail. The kinetics and isotherm study showed the adsorption of Orange II on MNPs/MgAl-LDH obeyed the pseudo-second-order and Langmuir model respectively and the adsorption processes were spontaneous and endothermic in nature. Also, some coexisting anions such as Cl^-, NO_3^-, CO_3^- and SO_4^{2-} had no significant effect on the removal of Orange II. The mechanism study revealed that the adsorption of Orange II on MNPs/MgAl-LDH mainly involves surface adsorption through electrostatic force and the layer anion exchange. Moreover, Orange II could be desorbed from MNPs/MgAl-LDH using 100 mg L^{-1} NaOH and used for four cycles without any adsorption performance loss, demonstrating MNPs/MgAl-LDH prepared in this work could be used as a cost-effective and efficient material for the removal of Orange II.

Key words | adsorption, layered double hydroxide, magnetic nanoparticles, Orange II

Bo Zhu
Lixian Chen
Tianyi Yan
Jiangyan Xu
Yanyu Wang
Min Chen
Hongmei Jiang (corresponding author)
College of Science,
Nanjing Agricultural University,
Weigang, Nanjing,
China
E-mail: *jianghongmei@njau.edu.cn*

INTRODUCTION

Azo dyes have been widely used in textile, cosmetic, paper, leather, paint, pigment and food industries, thus producing large volumes of wastewater with strong color and high concentration of organics and inorganics (Sharma *et al.* 2011). As a typical azo dye containing one azo bond (–N=N–), Orange II is known to be non-biodegradable due to its large aromatic structure that offers high degree of chemical, biological and photocatalytic stability (Zhou *et al.* 2016). In addition, Orange II is highly toxic and carcinogenic and the presence of it in wastewater can also lead to high chemical oxidation demand and an unpleasant odor (Luo *et al.* 2016). Therefore, it is very important to look for efficient technologies for the removal of Orange II from aquatic systems.

Up to now, a variety of techniques have been applied for removing Orange II such as membrane separation process (Yang *et al.* 2017), electrochemical treatment (Brillas & Martínez-Huitle 2015), and adsorption (Asgher 2012; Reddy & Lee 2013; Kyzas & Kostoglou 2014). Owing to low cost, easy operation, high efficiency, simplicity of the equipment and excellent regeneration ability, adsorption appears to be a promising method for the removal of dyes. The focus of the adsorption technique rests with the efficiency and effectiveness of the adsorbent, which depend on high surface areas and numerous binding sites of the adsorbents. Currently, a series of adsorbents, such as activated carbon (Mezohegyi *et al.* 2012), agricultural waste (Salleh *et al.* 2011), cellulose and chitosan (Oliveraa *et al.* 2016), graphene (Chowdhury & Balasubramanian 2014), carbon nanotubes (Yu *et al.* 2014) and other nanomaterials (Tan *et al.* 2015), have been employed for the treatment of dye wastewater. However, when using these adsorbents, it is time-consuming

doi: 10.2166/wst.2018.388

and inconvenient to separate the liquids from the solids by centrifugation.

Recently, there has been an increasing attention on magnetic iron or iron oxide nanoparticles for water treatments due to their fast separation and high convenience (Xu *et al.* 2012). The adsorption capacity of naked magnetic iron oxide nanoparticles is relatively small and the nanoparticles tend to aggregate because of high surface free energy; thus surface modification is considered to be an effective method to stabilize these naked magnetic materials, improve their adsorption performance and extend their application (Alqadami *et al.* 2017a, 2017b).

Layered double hydroxides (LDHs), such as well-known hydrotalcite-like anionic clays, have been widely used as adsorbent for the removal of dye from the wastewater due to their special layered structure, positively charged surface and unique anion exchange property of their host anion (Zhu *et al.* 2016). The combination of LDHs with magnetic particles would efficiently improve the separation property of LDHs and effectively raise the adsorption performance of magnetic particles. Several groups have reported some novel magnetic-core/LDH-shell hierarchical structures (MNP@LDH) and applied them for the separation of some pollutants (Shao *et al.* 2012; Zhang *et al.* 2013a, 2013b; Jiao *et al.* 2014; Shan *et al.* 2014; Zhang *et al.* 2015; Wu *et al.* 2017). In their studies, MNP@LDH can be fabricated by co-precipitating divalent and trivalent metal ions on the surface of MNP in alkaline medium, leading to the interface nucleation and crystal growth of LDHs (Jiao *et al.* 2014; Shan *et al.* 2014; Zhang *et al.* 2013a; Wu *et al.* 2017). In order to control the structure, size and morphology of MNP@LDH precisely, MNP can be coated with a thin carbon (MNP@C) or silica (MNP@SiO_2) layer first and then coated with -AlOOH, and in the end MNP@C@LDH or MNP@SiO_2@LDH can be synthesized by an *in situ* growth technique in a solution containing the appropriate cations. Also these delicate preparation methods for core-shell magnetic composites, MNP-LDH nanohybrids can be designed into a non-core-shell structure via an electrostatic interaction, reported by Chen *et al.* (2011, 2012), which is more convenient. However, LDH layers are prepared by both precipitation and co-precipitation methods not only in core-shell structure but also in non-core-shell structure, which forms varying sizes and large aggregates of sheet-like LDH nanocrystallites.

Herein, we propose a simple and efficient method to prepare a nanohybrid of magnetic Fe_3O_4 (MNPs) and MgAl-LDH (MNPs/MgAl-LDH) via electrostatic interaction and, more importantly, LDHs are prepared by urea hydrolysis reaction under hydrothermal conditions, which can contribute to a uniform and well-crystallized structure. Also, the newly prepared materials are used to remove Orange II from an aquatic system and the effects of different parameters on adsorption capacity of Orange II (pH, the initial concentrations of Orange II, temperature, competing anions) are investigated in detail. In addition, isotherms, kinetics, thermodynamics, desorption and regeneration are all studied. Furthermore, the adsorption mechanism of Orange II on MNPs/MgAl-LDH is extrapolated through zeta potential and Fourier transform infrared (FT-IR) analysis.

MATERIALS AND METHODS

Materials

Orange II, $FeCl_3{\cdot}6H_2O$, $Mg(NO_3)_2{\cdot}6H_2O$, and $A1(NO_3)_3{\cdot}9H_2O$ were bought from Bodi Chem. Co. Ltd (Tianjing, China). NaOH, Na_2CO_3, $NaNO_3$, Na_2SO_4, Na_3PO_4, NaCl, $NH_3{\cdot}H_2O$ and HCl were all purchased from Taishan Chem. Co. Ltd (Guangzhou, China). Anhydrous sodium acetate, ethanol and ethylene glycol were analytical grade and commercially available products.

Synthesis of MNPs

The preparation of MNPs was as the same as our previous work (Jiang *et al.* 2016). Briefly, $FeCl_3{\cdot}6H_2O$, ethylene glycol and NaAc were mixed together and stirred until a clear solution was formed. And then the mixture was transfered into a Teflon stainless steel autoclave, sealed and heated at 198 °C for 8 h.

Synthesis of magnetic MNPs/MgAl-LDH

First, 0.41 g $Mg(NO_3)_2{\cdot}6H_2O$ and 0.3 g $Al(NO_3)_3{\cdot}9H_2O$ were dissolved in deionized water. After the solution was ultrasonicated for 10 min, 0.336 g urea and 0.1 g MNPs were added into the mixed solution successively, then ultrasonicated to obtain a homogeneous solution and the solution was transferred into a Teflon stainless steel autoclave, sealed and heated 150 °C for 6 h. The obtained product was separated by a permanent magnet. The MNPs/MgAl-LDH was washed three times with ethanol and dried at room temperature.

Characterization methods

Morphologies and structure images of MNPs and MNPs/MgAl-LDH composite were obtained with a JEM-200CX transmission electron microscope (JEOL, Tokyo, Japan) and ARL X'TRA X-ray diffractometer (ARL, Lausanne, Switzerland). FT-IR spectra were recorded in the range from 4,000 to 400 cm^{-1} using the KBr pellet technique by a TENSOR27FT-IR (Bruker, Germany). The surface zeta potentials of the materials were measured using a zeta potential analyzer (Zeta PALS, Brookhaven Instruments Co., USA). The pH values were adjusted by a Mettler Toledo FE20 pH meter (Mettler-Toledo, Shanghai, China) supplied with a combined electrode. A KQ3200DE ultrasonic bath (Kunshan Shumei Ultrasonic Instrument, Suzhou, China) was applied to speed up the adsorption process.

Adsorption experiments

Adsorption processes were carried out using the typical batch method. First, 0.02 g adsorbents and 10 mL Orange II solution were added into in a 25 mL beaker and the mixture was adjusted to the desired pH with 0.1 mol L^{-1} HCl and $NH_3{\cdot}H_2O$. After being placed in an ultrasonic bath (40 kHz of ultrasound frequency and 100 W of power) to accelerate adsorption for 5–100 min, the solution was separated by magnetic separation. Then, the residual dyes in the beaker were measured by a spectrophotometer at a wavelength of maximum absorbance of 484 nm.

The effects of pH (2–8), the initial dye concentration (5–120 mg L^{-1}), contact time (5–100 min), temperature (298, 308, and 318 K) and the coexisting anions (Cl^-, NO_3^-, CO_3^-, SO_4^{2-} and PO_4^{3-}) on the adsorption of Orange II on the adsorbents were examined. In addition, not only an adsorption equilibrium study but also the kinetics study for the adsorption of Orange II was carried out. All experiments were duplicated and the average value is reported. The removal efficiency (R%) and the adsorption capacity(Q, mg g^{-1}) for Orange II were evaluated from the following formulas:

$$R\% = \frac{(C_o - C_e)}{C_o} * 100\% \quad (1)$$

$$Q = \frac{(C_o - C_e)V}{M} \quad (2)$$

where C_o and C_e (mg L^{-1}) are the initial and equilibrium concentration of Orange II respectively, V (L) is the volume of the adsorbate solution, M (g) is the mass of adsorbent.

Desorption and regeneration experiments

Typically, 20 mg Orange II-loaded adsorbents were ultrasonically treated in the presence of 10 mL of 100 mg L^{-1} NaOH for 15 min. After being magnetically separated, the adsorbent was washed with deionized water for three times and then directly used for the next cycle. Five sequential cycles of adsorption–desorption were carried out. The desorption percentage (D%) of Orange II was calculated using the following equation:

$$D = \frac{C_d}{C_o} * 100\% \quad (3)$$

where C_o and C_d are concentration of Orange II (mg L^{-1}) in the initial solutions and in the desorption solutions, respectively.

RESULTS AND DISCUSSION

Characterization of the MNPs/MgAl-LDH composite

SEM images

The morphology and structural features were examined by scanning electron microscopy (SEM) and the images of MNPs and MNPs/MgAl-LDH are shown in Figure 1. As observed, the naked MNPs were almost uniform and spherical in shape with a diameter of about 200 nm, while the morphology of MNPs/MgAl-LDH became a composite of spheric shape and regular hexagon. According to Toshiyuki (cited in Hibino & Ohya (2009)), orthohexagonal shape MgAl-LDH could be obtained using urea hydrolysis reaction under hydrothermal conditions, which suggested the successful fabricating of MNPs/MgAl-LDH.

XRD pattern

The crystalline structure of both MNPs and MNPs/MgAl-LDH was determined by X-ray diffraction (XRD) and is illustrated in Figure 2. The diffraction peaks with 2θ at 30.4°, 35.6°, 43.3°, 57.3°, and 62.8° shown in both materials can be indexed as a face-entered cubic Fe_3O_4 phase, which confirmed that the crystalline structure of MNPs was not affected by the introduction of MgAl-LDH. Another two new peaks appearing at 11.6° and 23.4° displayed only in the curve of MNPs/MgAl-LDH were ascribed to the characteristic reflections of LDH. These results demonstrated that the compounds of

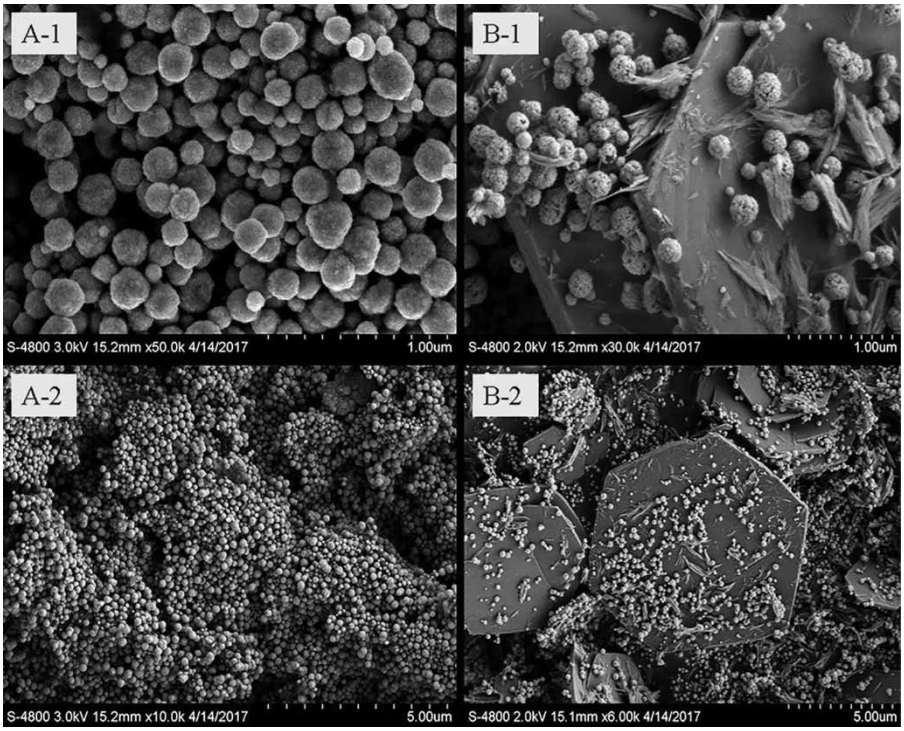

Figure 1 | SEM images of MNPs (A-1 and A-2) MNPs/MgAl-LDH (B-1 and B-2).

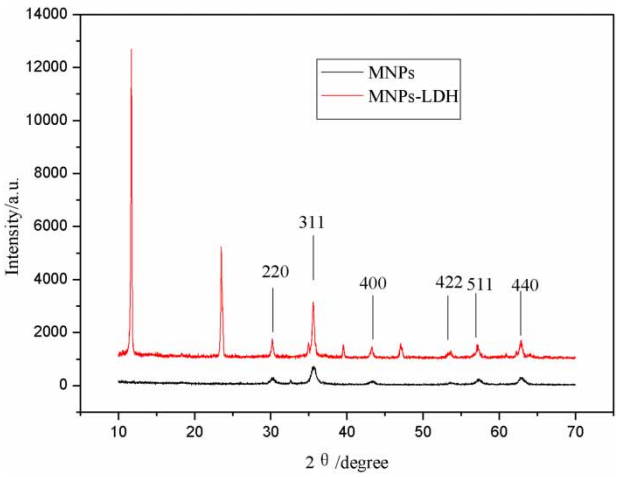

Figure 2 | XRD pattern of MNPs and MNPs/MgAl-LDH.

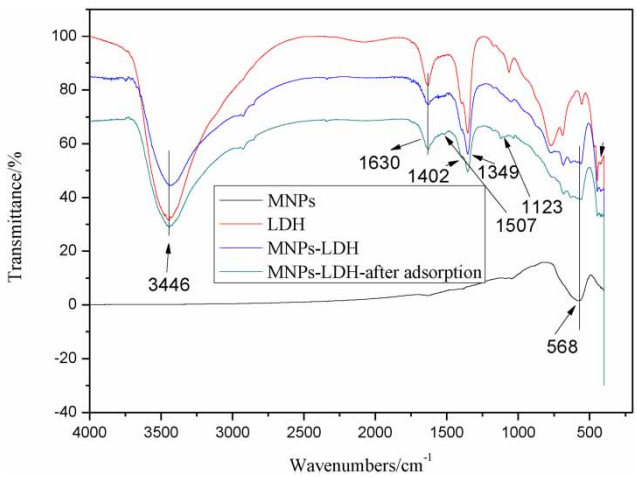

Figure 3 | IR spectra of MNPs and MNPs/MgAl-LDH.

MNPs/MgAl-LDH have been prepared successfully, which was in good agreement with the results in SEM images.

FT-IR spectra

The FT-IR spectra of MNPs, LDH and MNPs/MgAl-LDH are displayed in Figure 3. As observed, an absorption peak at 568 cm^{-1} can be seen on both MNPs and MNPs/MgAl-LDH, which corresponds to the Fe–O bonds (Chen *et al.* 2012; Jiang *et al.* 2012). The absorption peaks at 772 cm^{-1} and 689 cm^{-1} exhibited in the spectra of LDH and MNPs/MgAl-LDH may be associated with Mg-O-Al or O-Mg-O lattice vibrations (Shou *et al.* 2015). The strong peak at 1,349 cm^{-1} shown in the spectra of LDH and MNPs/MgAl-LDH came from the interlayer carbonate species (Zhang *et al.* 2013b; Wu *et al.* 2017). Also, there was a wide band around 3,446 cm^{-1} in the above spectra, which was ascribed to hydroxyl stretching mode from LDH layers and interlayer water molecules (Zhang *et al.* 2015). And an intense band at 1,630 cm^{-1} in the above spectra was

attributed to the hydroxyl deformation mode of the water molecules in the interlayer (Chen *et al.* 2011; Zhang *et al.* 2013b). All these results confirmed that the composite of MNPs/MgAl-LDH have been successfully prepared.

Magnetic analysis

To evaluate the magnetic properties, the naked MNPs/MgAl-LDH and the used MNPs/MgAl-LDH were studied by a vibrating sample magnetometer at room temperature. The results showed that both of the materials were essentially superparamagnetic and the saturation magnetization values of the naked MNPs/MgAl-LDH and the used MNPs/MgAl-LDH were 48 emu g^{-1} and 42.8 emu g^{-1} respectively, which suggested that the adsorption process has little impact on the magnetism of adsorbent.

Adsorption studies

Effect of pH

The pH of the system has profound influence on the adsorption of dyes in aqueous solution because it decides not only the existing form of the dyes but also the degree of protonation of functional groups on the surface of adsorbents. The influence of acidity on the adsorption of dye on MNPs and MNPs/MgAl-LDH was investigated in the pH range from 2 to 8 and the results are shown in Figure 4. It can be seen that the adsorption capacity of Orange II on MNPs/MgAl-LDH increased rapidly as pH was increased from 2 to 3 and then remained unchanged. When pH was higher than 4, the adsorption capacity of Orange II on MNPs/MgAl-LDH decreased significantly, whereas the adsorption capacity of Orange II on MNPs showed almost no change during the whole pH range and it was only about 5 mg g^{-1}. Also, from the two curves, it can be seen that the introduction of LDH can contribute to the adsorption capacity of Orange II remarkably. According to these results, pH 3.5 was selected for further experiments.

Adsorption equilibrium

The effect of initial concentration of Orange II, ranging from 5 to 120 mg L^{-1}, on the adsorption capacity of Orange II on MNPs and MNPs/MgAl-LDH was evaluated and the results are shown in Figure 5. As revealed, the adsorption capacity of Orange II on MNPs/MgAl-LDH increased rapidly first and then reached the maximum of 140 mg g^{-1}. The speedy adsorption during lower initial concentrations was assigned to abundant available active sites on the surface of the adsorbent and free Orange II, which facilitated the adsorption promptly. With the increasing concentration of Orange II and exhausting of active sites on the surface of adsorbents, Orange II in the solution could only react with inner active sites, resulting in a slow adsorption progress and long equilibrium adsorption time. In comparison with the uptake of Orange II on MNPs/MgAl-LDH (140 mg g^{-1}), the saturated uptake of Orange II on MNPs was only about 18 mg g^{-1}, which revealed the effective introduction of LDH on MNPs.

Isotherm studies can describe how the adsorbate interacts with the adsorbents and provide the distribution of

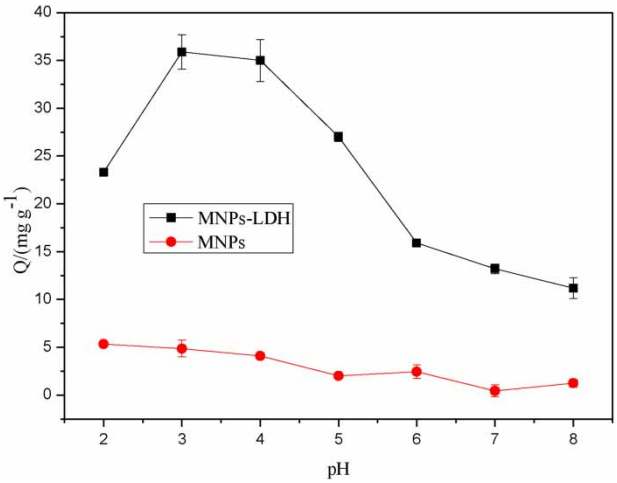

Figure 4 | Effects of pH on the adsorption capacity of Orange II on MNPs and MNPs/MgAl-LDH. C_o: 10 μg mL^{-1}, *V*: 10 mL, *M*: 2 mg, time: 15 min, *T*: 25 °C.

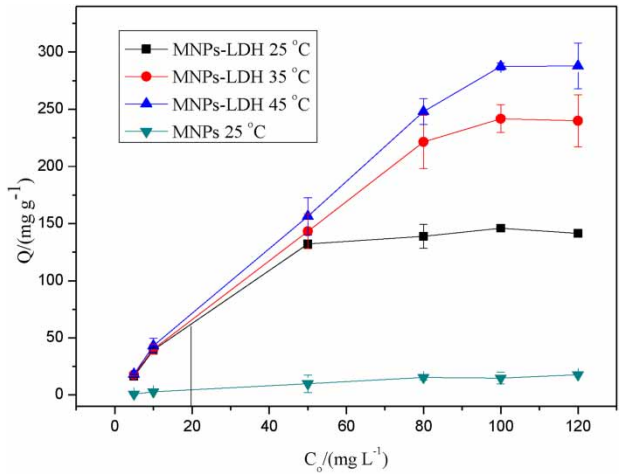

Figure 5 | Effects of initial Orange II concentration on the adsorption capacity of Orange II on MNPs/MgAl-LDH under different temperatures. pH: 3.5, *V*: 10 mL, *M*: 2 mg, time: 50 min.

adsorbate between the solid and liquid phase when the adsorption reaches the equilibrium. The well-known Langmuir isotherm model in Equation (4) was used to predict the experimental isotherms.

$$\frac{C_e}{q_e} = \frac{1}{K_L Q_{max}} + \frac{C_e}{Q_{max}} \quad (4)$$

where Q_{max} (mg g^{-1}) is the maximum adsorption capacity, C_e (mg L^{-1}) is the equilibrium concentration of Orange II in the solution, q_e (mg g^{-1}) is the equilibrium adsorption capacity, K_L (L mg^{-1}) is the Langmuir constant.

The Langmuir isotherm model assumes that one site can only be occupied by one molecule, the adsorption site is homogeneous and there is no interaction between the adsorbed molecules (Wang *et al.* 2014). The values of Q_{max} and K_L can be calculated from the slope and intercept of the plot of C_e/q_e vs. C_e, and the fitting parameters are summarized in Table 1. As observed, high correlation coefficients of the Langmuir equation could be acquired, suggesting the monolayer adsorption of Orange II on MNPs/MgAl-LDH. Also, the maximum adsorption capacity of Orange II on MNPs/MgAl-LDH was 149 mg g^{-1} at 298 K, which was much higher than that on MNPs and in good agreement with the experimental results. In order to know the superiority of our adsorbent, we have compared the adsorption capacity of the material prepared in this work with other material reported in the references and listed them in Table 2. As can be seen from Table 2, our adsorbent has a higher adsorption capacity than most of the other adsorbents.

Adsorption kinetics

The effects of adsorption time on the adsorption of Orange II on MNPs/MgAl-LDH are shown in Figure 6. The results exhibited that a fast adsorption process for Orange II happened during the first minutes and then reached equilibrium adsorption, which was possible due to the large quantity of active binding sites of the adsorbents in the first stage and the decreased active sites with the increasing of adsorbing time. In addition, the equilibrium adsorption time and equilibrium adsorption capacity were about 15 min and 41.7 mg g^{-1} for 10 mg L^{-1} Orange II, 30 min and 55.7 mg g^{-1} for 20 mg L^{-1} Orange II and 50 min and 154.8 mg g^{-1} for 150 mg L^{-1} Orange II respectively. This was because the higher initial concentration of

Table 1 | Langmuir parameters for the adsorption of Orange II on MNPs/MgAl-LDH

	Langmuir parameters		
Materials	**q_e (mg g^{-1})**	**K_L (L mg^{-1})**	**R^2**
Fe_3O_4 (25 °C)	27	0.0124	0.99
Fe_3O_4/MgAl-LDH (25 °C)	149	0.2621	0.99
Fe_3O_4/MgAl-LDH (35 °C)	286	0.0836	0.99
Fe_3O_4/MgAl-LDH(45 °C)	323	0.1164	0.99

Table 2 | Comparison of adsorption capacity of Orange II on different adsorbents

Adsorbents	Absorption capacity (mg g^{-1})	Reference
CTAB-modified cornstalk biochar	29.1	Mi *et al.* (2016)
Core/shell nanoadsorbent based on Fe_3O_4 magnetic nanoparticles surface-modified with a copolymer using 2, 4-diaminophenol and formaldehyde	121.07	Huo *et al.* (2018)
Magnetic polymer multi-wall carbon nanotube	67.57	Gao *et al.* (2013)
Banana peel-activated carbon	333	Ma *et al.* (2015)
Phosphonium-modified Algerian bentonites	53.78	Bouzid *et al.* (2015)
Chemically modified masau stones	136.8	Albadarin *et al.* (2017)
Fe_3O_4/MgAl-layered double hydroxide magnetic composites	323	This work

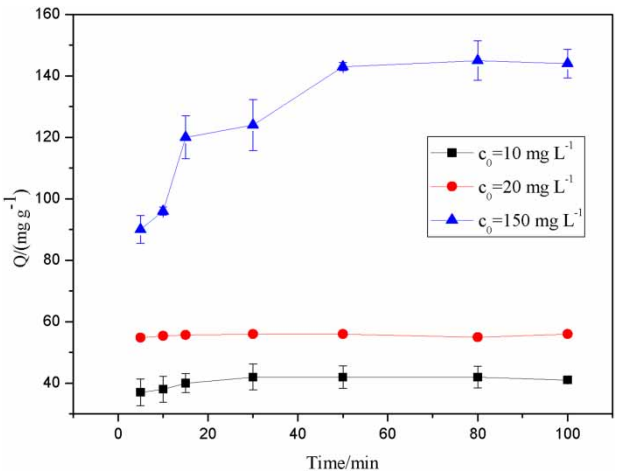

Figure 6 | Effects of contact time on the adsorption capacity of Orange II on MNPs/MgAl-LDH under three different initial Orange II concentrations. pH: 3.5, *V*: 10 mL, *M*: 2 mg, *T*: 25 °C.

analyte could provide more analyte, which could react with not only the surface active sites but also the inside active sites, leading to a shorter time for equilibrium and higher adsorption capacity.

In order to further elucidate the adsorption process, the pseudo-second-order kinetics model, based on the assumption that chemisorption is the rate determining step, was chosen to fit adsorption data in this work and was expressed as Equation (5)

$$\frac{t}{q_t} = \frac{1}{K_2 q_e^2} + \frac{t}{q_e} \tag{5}$$

where q_t (g mg^{-1}) and q_e (g mg^{-1}) represent the adsorption capacity at time t (min) and equilibrium, respectively, and K_2 (g (mg min)$^{-1}$) is the second-order rate constant.

Kinetic parameters were generated from the slope and intercepts of the linear plots of t/q_t against t and are summarized in Table 3. It was found that the experimental q_e value of 144 mg g^{-1} was consistent with the q_e value of 154 mg g^{-1} calculated from the pseudo-second-order model. Also, the high correlation coefficient of 0.99 for all three initial concentrations of Orange II were obtained, indicating that the pseudo-second-order model fitted the adsorption kinetics of Orange II well.

Thermodynamic study

The adsorption thermodynamic study is usually examined from the adsorption isotherms at different temperatures, and the thermodynamic parameters such as Gibbs free energy (ΔG^0, kJ mol^{-1}), enthalpy (ΔH^0, kJ mol^{-1}) and entropy (ΔS^0, J mol^{-1} K^{-1}) are calculated using the following equations:

$$\Delta G^0 = -RT\ln K_d \tag{6}$$

$$\ln K_d = \frac{\Delta S^0}{R} - \frac{\Delta H^0}{RT} \tag{7}$$

where R is the universal gas constant (8.314 J mol^{-1} K^{-1}) and T is the absolute temperature (K). K_d denotes the distribution constant of the adsorption process and can be calculated according to the method of Lyubchik and colleagues (Rajabi *et al.* 2016) by plotting $\ln(q_e/c_e)$ vs. q_e for different temperatures and extrapolating q_e to zero. The linear plot of $\ln K_d$ vs. $1/T$ yields a slope of $\Delta H/R$ and an intercept of $\Delta S/R$ and the results are presented in Table 4.

The values of ΔG were found to be negative at all three temperatures, suggesting the spontaneous nature of the adsorption process. Moreover, the values of ΔG decreased with the increase of temperature, which was in good agreement with the increasing adsorption capacity. The positive value of ΔH and ΔS reflected an endothermic nature and an increased randomness at the solid–solution interface during the adsorption process. These results demonstrated that chemical reaction or bonding was involved in the adsorption process.

Effect of coexisting anions

There are a number of anions in natural water and industrial wastewater, which would compete for adsorption sites and influence the removal efficiency of the adsorbent. The effects of common coexisting anions such as Cl^-, NO_3^-, CO_3^-, SO_4^{2-} and PO_4^{3-} on the adsorption capacity of Orange II on MNPs/MgAl-LDH were investigated and the results are presented in Figure 7. Evidently, the presence of the above coexisting anions except PO_4^{3-} has no significant effect on adsorption of Orange II. Generally, the higher electric charge and smaller radius will lead to larger affinity between the analytes and adsorbents (Zhao *et al.* 2010), leading to the severe inhibition of adsorption of Orange II by PO_4^{3-}. Owing to the low concentration range of phosphate in natural water (0–5 mg L^{-1}) (Chai *et al.* 2013), the interference from phosphate would be not as strong as shown in this study. The above results revealed that MNPs/MgAl-LDH owned a high selectivity and affinity toward Orange II, further indicating that it was a very efficient and promising adsorbent for the removal of Orange II.

Table 3 | Pseudo-second-order parameters of the adsorption of Orange II on MNPs/MgAl-LDH

	Pseudo-second-order parameters		
Initial concentration (μg mL^{-1})	q_e (mg·g^{-1})	K_2 (g (mg min)$^{-1}$)	R^2
10	41.67	0.06544	0.99
20	55.68	1.5316	0.99
100	154.8	0.001033	0.99

Table 4 | Thermodynamic parameters for the adsorption of Orange II on MNPs/MgAl-LDH

T (K)	q_e (mg g^{-1})	ΔG^0 (kJ mol^{-1})	ΔH^0 (kJ mol^{-1})	ΔS^0 (J mol^{-1} K^{-1})
298	149	−14.84	1.72	17.38
308	286	−14.57		
318	323	−13.28		

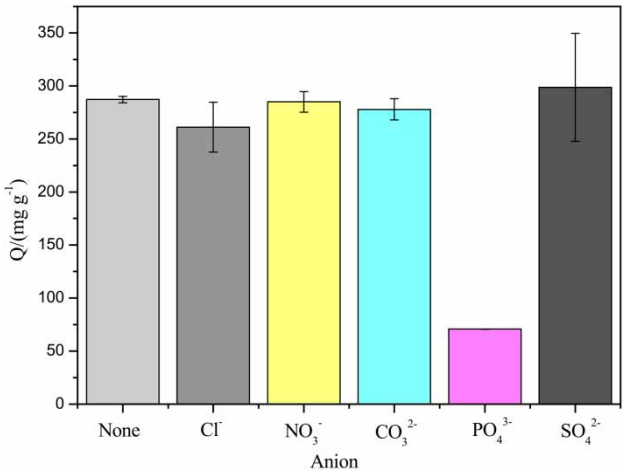

Figure 7 | Effects of coexisting anions on the adsorption capacity of Orange II on MNPs/MgAl-LDH. pH: 3.5, *V*: 10 mL, *M*: 2 mg, *T*: 45 °C, $C_{o(Orange\ II)}$: 100 μg mL^{-1}, $C_{o(coexisting\ anions)}$: 100 μg mL^{-1}.

Adsorption mechanisms

Based on the foregoing results, the adsorption capacity of Orange II on MNPs/MgAl-LDH was much higher than that on MNPs, displaying that MgAl-LDH was mostly responsible for the removal of Orange II. For the purpose of explaining the adsorption mechanism, zeta potential and FT-IR analyses were performed. As observed in Figure 8, the isoelectric point (pHpzc; pzc: point of zero charge) of MNPs/MgAl-LDH before adsorption was 8.66 and declined to 8.0 after adsorption. This meant that when pH value was lower than pHpzc of MNPs/MgAl-LDH, the surface of adsorbents would charge positively due to the protonation of hydroxyl groups on the outer layer of MgAl-LDH and would tend to adsorb anion dye Orange II through electrostatic attraction, contributing to a high adsorption capacity. At pH values higher than pHpzc, MNPs/MgAl-LDH would charge negatively due to the deprotonation of hydroxyl groups and thus generate electrostatic repulsion between the adsorbents and analytes, resulting in a lower adsorption capacity of Orange II. Hence, the absorption of Orange II on the external surface and the edge of MNPs/MgAl-LDH through electrostatic interactions can contribute to a very high adsorption performance of Orange II (Gao *et al.* 2014).

In addition, the pHpzc shifted from 8.66 to 8.0 after dye adsorption, implying there was some other adsorption mechanism also electrostatic force adsorption. Comparing the IR spectra before adsorption and after adsorption shown in Figure 3, the intensity of the characteristic peak of CO_3^{2-}, appearing at about 1,349 cm^{-1}, decreased visibly, indicating part of CO_3^{2-} had been replaced by anionic dye that was from the dissociated sulfonate groups of Orange II via anion exchange. Moreover, two new peaks at 1,123 cm^{-1} and 1,507 cm^{-1} that belong to Orange II arose in the spectrum of MNPs/MgAl-LDH after adsorption (Lua *et al.* 2017), revealing that anionic dye might enter into the interior of MNPs/MgAl-LDH.

Taking account of the above results and conclusion, the adsorption mechanism was possibly based on the following two steps: surface adsorption through electrostatic force and the layer anion exchange, which is in good agreement with some other reports (Shan *et al.* 2014).

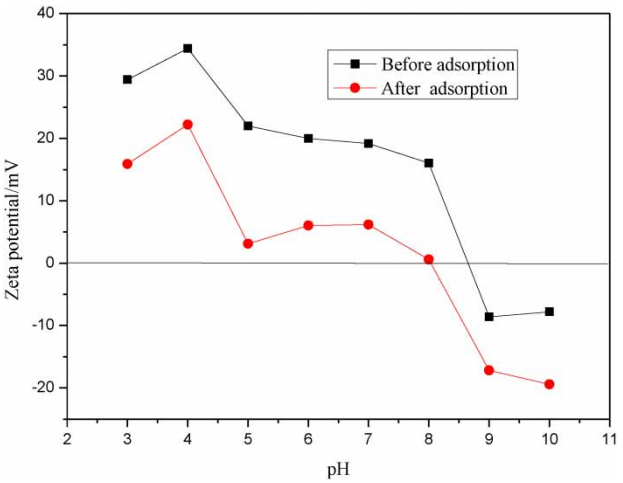

Figure 8 | Zeta potentials of MNPs/MgAl-LDH before adsorption and after adsorption.

Desorption and regeneration

The stability and regeneration potential of the adsorbent are very important for its practical application, so the desorption experiments were carried out. Considering that the adsorption of Orange II is very low in an alkaline medium, NaOH was used to attempt to desorb Orange II from the adsorbents in this work. The results showed that the desorption rate could be still over 85% after at least four cycles using 0.1 mol L^{-1} NaOH as desorption reagent, illustrating that MNPs/MgAl-LDH had good stability and reusability.

CONCLUSION

An efficient MNPs/MgAl-LDH composite with excellent adsorption performance and superparamagnetism property has been successfully synthesized by a two-step hydrothermal method combined with the urea hydrolysis reaction.

The SEM, XRD and FT-IR results indicated that spheric shape MNPs and regular hexagon MgAl-LDH have been combined very well through physical adsorption. The composite exhibited a high adsorption capacity of 149 mg g^{-1} under 25 °C and 323 mg g^{-1} under 45 °C towards Orange II, while the adsorption capacity of Orange II on pure MNPs was only 27 mg g^{-1}). The adsorption process of the Orange II on MNPs/MgAl-LDH was also systematically investigated, demonstrating that it followed the pseudo-second-order model and the Langmuir monolayer model and was spontaneous and endothermic in nature. The presence of commonly coexisting anions in solution had no remarkable influence on the removal of Orange II, displaying the high selectivity for Orange II. Furthermore, the mechanisms study illustrated the two main adsorption mechanisms: surface adsorption through electrostatic force and the layer anion exchange during the adsorption of Orange II on MNPs/MgAl-LDH. Finally, Orange II could be reused for four cycles without any adsorption performance loss using 100 mg L^{-1} NaOH as desorbing reagent, demonstrating that MNPs/MgAl-LDH prepared in this work would be a high efficient adsorbent for the removal of Orange II.

ACKNOWLEDGEMENT

Authors Bo Zhu and Lixian Chen are co-first author. They contributed equally to the present study. This work was supported by National Natural Science Foundation of China (21607075), and Fundamental Research Funds for the Central Universities (KJQN201721 and KYZ201600163).

REFERENCES

Albadarin, A. B., Solomon, S., Kurniawan, T. A., Mangwandi, C. & Walker, G. 2017 Single, simultaneous and consecutive biosorption of Cr(VI) and Orange II onto chemically modified masau stones. *Journal of Environmental Management* **204**, 365–374.

Alqadami, A. A., Naushad, M., Alothman, Z. A. & Ghfar, A. A. 2017a Novel metal–organic framework (MOF) based composite material for the sequestration of U(VI) and Th(IV) metal ions from aqueous environment. *ACS Applied Materials & Interfaces* **9** (41), 36026–36037.

Alqadami, A. A., Naushad, M., Abdalla, M. A., Ahamad, T., ALOthman, Z. A., Alsehri, S. M. & Ghfar, A. A. 2017b Efficient removal of toxic metal ions from wastewater using a recyclable nanocomposite: a study of adsorption parameters and interaction mechanism. *Journal of Cleaner Production* **156**, 426–436.

Asgher, M. 2012 Biosorption of reactive dyes: a review. *Water, Air and Soil Pollution* **223**, 2417–2435.

Bouzid, S., Khenifi, A., Bennabou, K. A., Trujilano, R., Vicente, M. A. & Derrich, Z. 2015 Removal of Orange II by phosphonium-modified Algerian bentonites. *Chemical Engineering Communications* **202**, 520–533.

Brillas, E. & Martínez-Huitle, C. 2015 Decontamination of wastewaters containing synthetic organic dyes by electrochemical methods. *Applied Catalysis B: Environmental* **166–167**, 603–643.

Chai, L. Y., Wang, Y. Y., Zhao, N., Yang, W. C. & You, X. Y. 2013 Sulfate-doped Fe_3O_4/Al_2O_3 nanoparticles as a novel adsorbent for fluoride removal from drinking water. *Water Research* **47**, 4040–4049.

Chen, C. P., Gunawan, P. & Xu, R. 2011 Self-assembled Fe_3O_4-layered double hydroxide colloidal nanohybrids with excellent performance for treatment of organic dyes in water. *Journal of Materials Chemistry* **21**, 1218–1225.

Chen, D., Li, Y., Zhang, J., Zhou, J. Z., Guo, Y. & Liu, H. 2012 Magnetic Fe_3O_4/ZnCr-layered double hydroxide composite with enhanced adsorption and photocatalytic activity. *Chemical Engineering Journal* **185–186**, 120–126.

Chowdhury, S. & Balasubramanian, R. 2014 Recent advances in the use of graphene-family nanoadsorbents for removal of toxic pollutants from wastewater. *Advances in Colloid and Interface Science* **204**, 35–56.

Gao, H., Zhao, S., Cheng, X., Wang, X. & Zheng, L. 2013 Removal of anionic azo dyes from aqueous solution using magnetic polymer multi-wall carbon nanotube nanocomposite as adsorbent. *Chemical Engineering Journal* **223**, 84–90.

Gao, C., Yu, X. Y., Luo, T., Jia, Y., Sun, B., Liu, J. H. & Huang, X. J. 2014 Millimeter-sized Mg-Al-LDH nanoflake impregnated magnetic alginate beads (LDH-n-MABs): a novel bio-based sorbent for the removal of fluoride in water. *Journal of Materials Chemistry A* **2**, 2119–2128.

Hibino, T. & Ohya, H. 2009 Synthesis of crystalline layered double hydroxides: precipitation by using urea hydrolysis and subsequent hydrothermal reactions in aqueous solutions. *Applied Clay Science* **45**, 123–132.

Huo, Y., Wu, H., Wang, Z., Wang, F., Liu, Y., Feng, Y. & Zhao, Y. 2018 Preparation of core/shell nanocomposite adsorbents based on amine polymer-modified magnetic materials for the efficient adsorption of anionic dyes. *Colloids and Surfaces A* **549**, 174–183.

Jiang, H. M., Yan, Z. P., Zhao, Y., Hu, X. & Lian, H. Z. 2012 Zincon-immobilized silica-coated magnetic Fe_3O_4 nanoparticles for solid-phase extraction and determination of trace lead in natural and drinking waters by graphite furnace atomic absorption spectrometry. *Talanta* **94**, 251–256.

Jiang, H. M., Sun, M. L., Xu, J. Y., Lu, A. M. & Shi, Y. 2016 Magnetic Fe_3O_4 nanoparticles modified with polyethyleneimine for the removal of Pb(II). *Clean – Soil Air Water* **44** (9999), 1–8.

Jiao, F. P., Yu, J. G., Song, H. L., Jiang, X. Y., Yang, H., Shi, S. Y., Chen, X. Q. & Yang, W. J. 2014 Excellent adsorption of Acid

Flavine 2G by MgAl-mixed metal oxides with magnetic iron oxide. *Applied Clay Science* **101**, 30–37.

Kyzas, G. Z. & Kostoglou, M. 2014 Green adsorbents for waste waters: a critical review. *Materials* **7**, 333–364.

Lua, L., Lia, J., Ng, D. H. L., Yanga, P., Songa, P. & Zuo, M. 2017 Synthesis of novel hierarchically porous Fe_3O_4@MgAl–LDH magnetic microspheres and its superb adsorption properties of dye from water. *Journal of Industrial and Engineering Chemistry* **46**, 315–323.

Luo, F., Yang, D., Chen, Z. L., Megharaj, M. & Naidu, R. 2016 One-step green synthesis of bimetallic Fe/Pd nanoparticles used to degrade Orange II. *Journal of Hazardous Materials* **303**, 145–153.

Ma, J., Huang, D., Zou, J., Li, L., Kong, Y. & Komarneni, S. 2015 Adsorption of methylene blue and Orange II pollutants on activated carbon prepared from banana peel. *Journal of Porous Materials* **22**, 301–311.

Mezohegyi, G., Van der Zee, F. P., Font, J., Fortuny, A. & Fabregat, A. 2012 Towards advanced aqueous dye removal processes: a short review on the versatile role of activated carbon. *Journal of Environmental Management* **102**, 148–164.

Mi, X., Li, G., Zhu, W. & Liu, L. 2016 Enhanced adsorption of Orange II using cationic surfactant modified biochar pyrolyzed from cornstalk. *Journal of Chemistry* DOI: 10.1155/2016/8457030.

Oliveraa, S., Muralidharab, H. B., Venkateshb, K., Gunab, V. K., Gopalakrishnab, K. & Kumar, K. Y. 2016 Potential applications of cellulose and chitosan nanoparticles/composites in wastewater treatment: a review. *Carbohydrate Polymers* **153**, 600–618.

Rajabi, H. R., Rajabi, S. R. H. R. & Razmpour, S. 2016 Synthesis, characterization and application of ion imprinted polymeric nanobeads for highly selective preconcentration and spectrophotometric determination of Ni^{2+} ion in water samples. *Spectrochimica Acta Part A: Molecular and Biomolecular Spectroscopy* **153**, 45–52.

Reddy, D. H. K. & Lee, S. M. 2013 Application of magnetic chitosan composites for the removal of toxic metal and dyes from aqueous solutions. *Advances in Colloid and Interface Science* **201–202**, 68–93.

Salleh, M. A. M., Mahmoud, D. K., Karim, W. A. W. A. & Idris, A. 2011 Cationic and anionic dye adsorption by agricultural solid wastes: a comprehensive review. *Desalination* **280**, 1–13.

Shan, R. R., Yan, L. G., Yang, K., Yu, S. J., Hao, Y. F., Yu, H. Q. & Du, B. 2014 Magnetic Fe_3O_4/MgAl-LDH composite for effective removal of three red dyes from aqueous solution. *Chemical Engineering Journal* **252**, 38–46.

Shao, M. F., Ning, F. Y., Zhao, J. W., Wei, M., Evans, D. G. & Duan, X. 2012 Preparation of Fe_3O_4@SiO_2@layered double hydroxide core-shell microspheres for magnetic separation of proteins. *Journal of the American Chemical Society* **134**, 1071–1077.

Sharma, P., Kaur, H., Sharma, M. & Sahore, V. 2011 A review on applicability of naturally available adsorbents for the removal of hazardous dyes from aqueous waste. *Environmental Monitoring and Assessment* **183**, 151–195.

Shou, J. X., Jiang, C. F., Wang, F., Qiu, M. Q. & Xu, Q. G. 2015 Fabrication of Fe_3O_4/MgAl-layered double hydroxide magnetic composites for the effective decontamination of Co(II) from synthetic wastewater. *Journal of Molecular Liquids* **207**, 216–223.

Tan, K. B., Vakili, M., Horri, B. A., Poh, P. E., Abdullah, A. Z. & Salamatinia, B. 2015 Adsorption of dyes by nanomaterials: recent developments and adsorption mechanisms. *Separation and Purification Technology* **150**, 229–242.

Wang, J. T., Ji, S. J., Ma, R. Y., Wu, Q. H., Wang, C., Qiang, J. & Wang, Z. 2014 Synthesis of magnetic Fe_3O_4 modified graphene nanocomposite and its application on the adsorption of some dyes from aqueous solution. *Separation Science and Technology* **49**, 861–867.

Wu, X. G., Li, B. & Wen, X. G. 2017 Synthesis and adsorption properties of hierarchical Fe_3O_4@MgAl-LDH magnetic microspheres. *Journal of Nanoparticle Research* **19**, 131.

Xu, P., Zeng, G. M., Huang, D. L., Feng, C. L., Hu, S., Zhao, M. H., Lai, C., Wei, Z., Huang, C., Xie, G. X. & Liu, Z. F. 2012 Use of iron oxide nanomaterials in wastewater treatment: a review. *Science of the Total Environment* **424**, 1–10.

Yang, L. B., Wang, Z. & Zhang, J. L. 2017 Zeolite imidazolate framework hybrid nanofiltration (NF) membranes with enhanced permselectivity for dye removal. *Journal of Membrane Science* **532**, 76–86.

Yu, J. G., Zhao, X. H., Yang, H., Chen, X. H., Yang, Q. Q., Yu, L. Y., Jiang, J. H. & Chen, X. Q. 2014 Aqueous adsorption and removal of organic contaminants by carbon nanotubes. *Science of the Total Environment* **482–483**, 241–251.

Zhang, H., Zhang, G. Y., Bi, X. & Chen, X. T. 2013a Facile assembly of a hierarchical core@shell Fe_3O_4@CuMgAl-LDH (layered double hydroxide) magnetic nanocatalyst for the hydroxylation of phenol. *Journal of Materials Chemistry A* **1**, 5934–5942.

Zhang, X. F., Wang, J., Li, R., Dai, Q. H., Gao, R., Liu, Q. & Zhang, M. L. 2013b Preparation of Fe_3O_4@C@layered double hydroxide composite for magnetic separation of uranium. *Industrial & Engineering Chemistry Research* **52**, 10152–10159.

Zhang, H., Huang, F., Liu, D. L. & Shi, P. 2015 Highly efficient removal of Cr(VI) from wastewater via adsorption with novel magnetic Fe_3O_4@C@MgAl-layered double-hydroxide. *Chinese Chemical Letters* **26**, 1137–1143.

Zhao, X. L., Wang, J. M., Wu, F. C., Wang, T., Cai, Y. Q., Shia, Y. L. & Jiang, G. B. 2010 Removal of fluoride from aqueous media by Fe_3O_4@$Al(OH)_3$ magnetic nanoparticles. *Journal of Hazardous Materials* **173**, 102–109.

Zhou, X. J., Shi, P. H., Qin, Y. F., Fan, J. C., Min, Y. L. & Yao, W. F. 2016 Synthesis of Co_3O_4/graphene composite catalysts through CTAB assisted method for Orange II degradation by activation of peroxymonosulfate. *Journal of Materials Science: Materials in Electronics* **27**, 1020–1030.

Zhu, Y. Z., Wang, F. H. & Zhang, C. 2016 Utilization of LDH-based materials as potential adsorbents and photocatalysts for the decontamination of dyes wastewater: a review. *RSC Advances* **83**, 79415–79436.

First received 20 March 2018; accepted in revised form 24 August 2018. Available online 5 September 2018